Applied Catalysis B: Environmental 100 (2010) 355–364

Contents lists available at ScienceDirect

Applied Catalysis B: Environmental

journal homepage: www.elsevier.com/locate/apcatb

Solvothermal synthesis of C–N codoped TiO_2 and photocatalytic evaluation for bisphenol A degradation using a visible-light irradiated LED photoreactor

Xiaoping Wang, Teik-Thye Lim*

Division of Environmental and Water Resources Engineering, School of Civil and Environmental Engineering, Nanyang Technological University, Block N1, 50 Nanyang Avenue, Singapore 639798, Singapore

ARTICLE INFO

Article history:
Received 27 April 2010
Received in revised form 2 August 2010
Accepted 8 August 2010
Available online 14 August 2010

Keywords:
C–N codoping
LED photoreactor
Bisphenol A
Solvothermal
Inorganic ions

ABSTRACT

In this study, a highly visible-light photoactive carbon and nitrogen codoped TiO_2 (CN-TiO_2) was synthesized via a facile solvothermal method. The conditions for each synthesis step including selection of dopants, solvothermal treatment, and calcination temperatures were evaluated. X-ray photoelectron spectroscopy shows that the surface of TiO_2 was modified by carbon and nitrogen via formation of Ti–C bonds, carbonate species and oxynitrides. The derived photocatalyst is predominantly of anatase phase, with well-developed mesoporosity and a large BET surface area (102 m^2/g). The photocatalytic degradation (PCD) of bisphenol A (BPA) by CN-TiO_2 was evaluated using a novel photoreactor irradiated with flexible strips of visible light-emitting diode (Vis-LED). The PCD of BPA was most favorable under circumneutral pH. Under 5 h of irradiation with white, blue, green and yellow LED lights, the extents of BPA degradation were >99%, >99%, 84% and 24% respectively, while the corresponding percentages of mineralization were 70%, 60%, 45% and 9%. Presence of sulfate, chloride and nitrate at 5.0 mM only slightly retarded BPA degradation, while bicarbonate and silica inhibited the process to a much larger extent. Deactivation of the CN-TiO_2 by silica could be attributed to the formation of surface-bound silica species. By adjusting to acidic condition, the detrimental effect from silica could be significantly suppressed.

1. Introduction

The heterogeneous photocatalysis has several advantages compared to other advanced oxidation processes in water treatment and purification, including avoiding the use of hazardous chemicals, minimum waste streams, energy efficient compared to photolysis and sonolysis, and operating under ambient condition. Photocatalysis with UV are able to degrade almost all organics except certain groups of perfluorinated chemicals [1]. TiO_2 is the most suitable photocatalyst for applications in water treatment due to its good photoactivity, high chemical and biological stability, relatively low cost, and low toxicity. However, its wide band gap energies of 3.2 and 3.0 eV, respectively for anatase and rutile phases require UV for photoexcitation.

Recently, significant efforts have been carried out to modify TiO_2 so that it can be photoresponsive under visible light in order to harness the major part of solar spectrum or to make use of interior lighting to power photocatalysis. Several approaches including doping of non-metals (C, N, F, S) [2–6] into TiO_2 have been developed to extend the absorption band-edge of TiO_2 to the visible-light region. Recently, it has been reported that codoping of TiO_2 with two or more elements, such as B–F, N–F, C–N, and S–N [7–12], could result in higher visible-light responses as compared to the TiO_2 doped with single element. For example, Li et al. [7] reported that N–F codoped TiO_2 prepared via spray pyrolysis exhibited higher photocatalytic decompositions of acetaldehyde and trichloroethylene compared to N-doped and F-doped TiO_2. They attributed the synergistic effect to the increased visible-light absorption, presence of surface oxygen vacancy, and formation of Ti^{3+} ions (promoted by F-doping). In another study, Chen et al. [10] prepared C–N codoped TiO_2 using sol–gel method which exhibited higher photocatalytic acidity under visible light compared to C-doped and N-doped TiO_2. They attributed this phenomenon to the enhanced adsorption to the carbonate species formed on the surface of the C–N codoped TiO_2 and visible-light photoactivity induced by N-doping into the TiO_2 lattice.

The solvothermal synthesis has been found to be a versatile route, which is controllable in synthesizing fine nanoparticles of high crystallinity with narrow size distribution at lower temperatures. The solvothermal method employed to synthesize nano-sized TiO_2 has been widely studied [13]. Solvothermal synthesis of N-doped TiO_2 photocatalysts has also been reported in several studies [14,15]. Yin et al. obtained N-doped TiO_2 by the homogeneous precipitation in hexamethylenetetramine–$TiCl_3$ followed by heat treatment under solvothermal conditions [16]. Furthermore, Huang et al. synthesized anatase type N–F codoped

* Corresponding author. Tel.: +65 6790 6933; fax: +65 6791 0676.
E-mail address: cttlim@ntu.edu.sg (T.-T. Lim).

0926-3373/$ – see front matter © 2010 Elsevier B.V. All rights reserved.
doi:10.1016/j.apcatb.2010.08.012

TiO_2 by a sol–gel-solvothermal method using triethylamine and ammonium fluoride as the source of dopants [17]. To our knowledge, simultaneous doping of TiO_2 with nitrogen and carbon via solvothermal synthesis has not been reported.

Development of LED (light-emitting diode)-based photoreactors has increasingly attracted research attention in recent years. The visible-LEDs (Vis-LED) are now widely used in outdoors and indoors lightings, and they can provide different lights of varying monochromatic wavelengths. The LED presents several merits, such as long lifetime, energy efficiency, high spectral purity, flexible configuration, and small footprint [18]. Because of its versatility, LED provides potential for inherently compact photoreactor designs and efficient optical solution in delivering energetic photons to the photocatalysts.

In this study, we have prepared a number of carbon and/or nitrogen doped TiO_2 via solvothermal method. Bisphenol A was the target pollutant to be degraded. It is an endocrine disrupter which has been widely used as a precursor in synthesis of epoxy resins and polycarbonate plastics [19] and is frequently found in urban wastewaters and treated effluents [20]. It represents a biorefractory and hydrophobic compound which cannot be removed in the conventional wastewater treatment processes. Nevertheless, it has been found amendable to photocatalytic degradation (PCD) under UV/TiO_2 [21–23]. To evaluate the action spectrum of the synthesized photocatalysts, different Vis-LEDs that emit white, blue, green and yellow lights were used as the excitation light sources. To examine the durability of the C–N codoped TiO_2 when used in treating real waters, the influence of pH and effects of several inorganic anions which are ubiquitous in natural waters and wastewaters were evaluated.

2. Experimental methods

2.1. Materials preparation

All chemicals used in the experiments were of analytical reagent grade without further purification. In a typical process, 5.96 mL of titanium isopropaoxide (TTIP) was dissolved in isopropanol (85 mL). 0.1 M HNO_3 (5 mL) and a known amount of hexamethylenetetramine (HMT) with the atomic ratio of Ti/N = 1 were added. The mixture was stirred continuously for 1 h at room temperature until a TiO_2 gel was obtained. Then the as-prepared TiO_2 gel was transferred into a 125 mL of Teflon-lined autoclave. The system was heated and maintained at a desired temperature (90, 120, or 160 °C) for 4 h. The product was separated by centrifugation, thoroughly washed with deionized water, dried at 90 °C overnight, and further calcined at a higher temperature for 4 h in a muffle furnace. Various samples were produced and denoted as CN-TiO_2(T_1/T_2), where T_1 and T_2 represent the temperatures of solvothermal treatment and calcination respectively. For comparison, CN-TiO_2(120/300)-U (using urea as the dopant source instead of HMT) and C-TiO_2(120/300) (without adding HMT, hereafter named as C-TiO_2) were also synthesized with the same procedure; the N-doped TiO_2 (N-TiO_2) was prepared by the homogenous precipitation-solvothermal process in $TiCl_3$-HMT aqueous and methanol solution following with calcination at 400 °C for 4 h [16].

2.2. Materials characterization

X-ray photoelectron spectroscopy (XPS) studies were carried out in an ultrahigh vacuum chamber with a base pressure below 2.66×10^{-7} Pa at room temperature. Photoemission spectra were recorded by a Kratos Axis Ultra spectrometer with a monochromatic Al Kα excitation source ($h\nu$ = 1486.71 eV). The binding energy (BE) scale was referenced to the C 1s core level at 248.8 eV of adventitious carbon. Curve fitting was performed using a mixed Gaussian–Lorenzian function with a Shirley background. Thermogravimetric analysis was performed on thermogravimetric analyzer (Perkin-Elmer) with a heating rate of 5 °C/min in an air flow. The UV–vis diffuse reflectance spectra were obtained using a UV–vis spectrometer (Lambda 35, Perkin-Elmer) equipped with an integrating sphere assembly. $BaSO_4$ was used as the reference. X-ray diffraction (XRD) patterns were collected by a Bruker D8 Advance X-ray diffractometer with monochromated high-intensity Cu Kα radiation (λ = 1.5418 Å) in a 2θ range of 5–80°. The particle morphology was observed with transmission electron microscopy (TEM, JEOL JEM-2010). The textual properties of samples were analyzed by N_2 adsorption/desorption at liquid-nitrogen temperature (77 K) using a Quantachrome Autosorb-1 system. The specific surface area was calculated using the Brunauer–Emmett–Teller (BET) equation, while the pore volume and pore size distribution were obtained from the Barrett–Joyner–Halenda (BJH) method from the N_2 adsorption isotherm. The zeta potential value was measured using a Malvern nano-zs zetasizer in suspension with photocatalyst concentration of 0.5 g/L. The pH was adjusted through addition of 0.05 M HCl or 0.05 M NaOH solution.

2.3. Photocatalytic activity evaluation

The photocatalytic degradation of bisphenol A was carried out in a Vis-LED photoreactor. It comprised a 500-mL borosilicate glass reactor and a 2-m flexible LED strip (SMD 5050, 30 pcs/m, 7.5 W/m) was wrapped around it (Fig. 1). Four different LED strips were used in this study, emitting blue light (main emission wavelength λ = 465 nm), green light (λ = 523 nm) and yellow light (λ = 589 nm), while spectrum of white LED clearly showed blue light emitted at about 450 nm and more broadband Stokes-shift light emitted at roughly 500–600 nm. A cooling jacket was wrapped around the photoreactor to maintain its temperature at 30 ± 5 °C throughout the running of the experiment. A mirror panel covered the reactor to minimize penetration of ambient light and water evaporation. The reaction solution was maintained under air-equilibrated conditions through slow bubbling.

Prior to the commencement of PCD experiments, a 400-mL suspension containing photocatalysts (dosage = 0.5 g/L) and BPA (5 ppm) was stirred in the dark for 1 h to attain adsorption/desorption equilibrium. At designated time intervals, aliquots of the solution filtered using cellulose acetate syringe membrane filters (Iwaki, 0.45 μm) were analyzed using a high-performance liquid chromatograph (HPLC, Perkin-Elmer Series200). The HPLC analysis was carried out using an Inertsil ODS-3 column and a Series 200 UV/Vis detector at 225 nm, with acetonitrile and water (70/30, v/v) as effluent at a flow rate of 1 mL/min. The total organic carbon (TOC) remaining in the solution was measured using a Shimadzu ASI-V TOC analyzer.

The effect of pH was also investigated through pH adjustment. The influence of anions on photocatalytic activities was examined by introducing appropriate amounts of Na_2SO_4, NaCl, $NaNO_3$, $NaHCO_3$, and Na_2SiO_3 salts into the suspension. It was observed that throughout the experiment, pH values of the solutions generally varied within a narrow range (less than 0.3 unit).

3. Results and discussion

3.1. XPS analysis

The XPS measurements were carried out to investigate the surface chemical compositions and bonding states of the as-prepared samples. The atomic concentrations of elements (Ti, N, O, C) present in the surface of as-prepared photocatalysts were calculated with

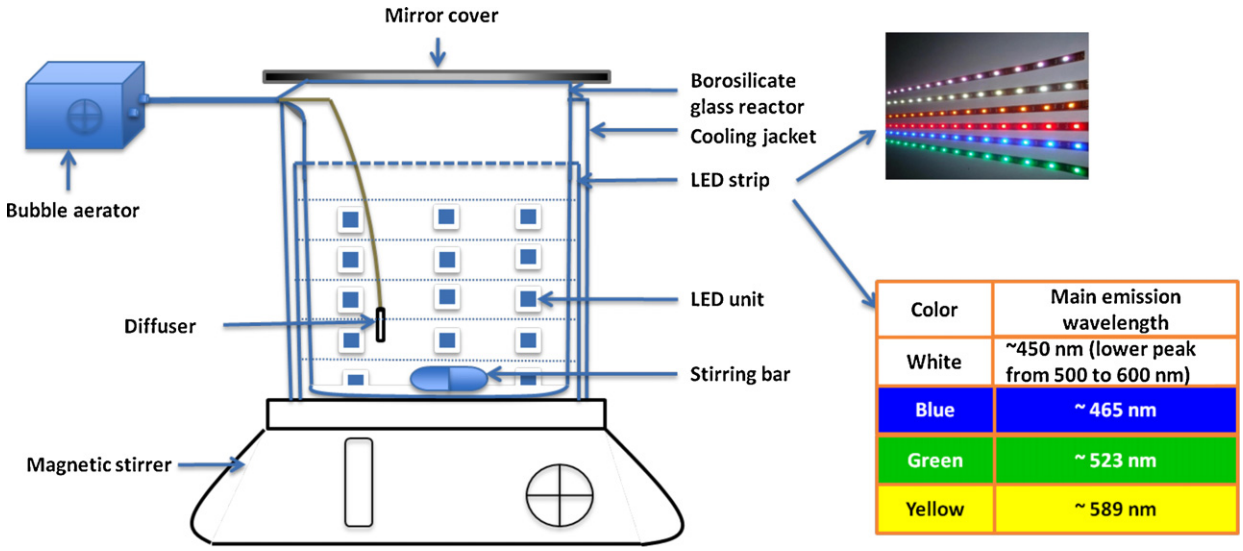

Fig. 1. Schematic diagram of photoreactor used for photodegradation of BPA with LED strips as excitation light source.

Table 1
Physicochemical properties of photocatalysts and their BPA and TOC removal efficiencies.

Photocatalyst	Atomic concentration (%)				Anatase size[b] (nm)	SSA[c] (m^2/g)	Band gap[d] (eV)	BPA removal at 2 h[e] (%)	TOC removal at 5 h[e] (%)
	Ti 2p	O 1s	N 1s	C 1s[a]					
CN-TiO_2(90/300)	23.92	61.23	0.18	14.67	9.3	105	2.96	36	27
CN-TiO_2(120/300)	19.10	63.60	0.83	16.47	10.7	102	2.80	96	70
CN-TiO_2(160/300)	15.97	60.26	0.67	23.10	13.3	92.8	2.90	64	55
CN-TiO_2(120/300)-U	23.69	63.24	0.24	12.83	9.8	96.6	2.99	67	54
CN-TiO_2(120/400)	21.58	62.86	0.44	15.12	13.1	90.2	2.95	29	25
CN-TiO_2(120/500)	24.58	67.27	0	8.15	14.8	47.5	3.02	23	20
CN-TiO_2(120/600)	26.38	68.36	0	5.26	27.3	34.3	3.04	14	20
C-TiO_2	23.42	62.25	0	14.33	8.2	156	3.05	64	56
N-TiO_2	26.39	69.31	3.26	1.04	6.7	143	2.92	29	28
P25	–	–	–	–	38.9	52.2	3.10	5	5

[a] Excluded adventitious carbon.
[b] Derived from XRD patterns.
[c] Specific surface area.
[d] Obtained from UV–vis spectra.
[e] Under white LED irradiation, neutral pH.

relative sensitivity factor (RSF) and listed in Table 1. The CN-TiO_2(120/300) contained the highest concentration of N (0.83%) among the samples obtained via solvothermal synthesis, while nitrogen was not detected in C-TiO_2, CN-TiO_2(120/500), and CN-TiO_2(120/600). 3.26% of N was present in N-TiO_2 synthesized by the homogenous precipitation–solvothermal process. For the atomic concentration of C, which excluded the adventitious carbon, it gradually decreased with the increasing calcination temperatures and could be negligible for the N-TiO_2.

The high-resolution scan over C 1s spectral regions are shown in Fig. 2. After fitting the XPS envelopes, the C 1s spectra of all samples share a common peak located at 284.8 eV, which is ascribed to adventitious carbon originating from the XPS instrument or carbon-containing species absorbed on the surface. As for CN-TiO_2(90/300), two additional peaks at 286.3 and 288.3 eV were observed. These peaks, around 286 and 288 eV, can be attributed to C–O and C=O bonds respectively, which suggests the formation of carbonate species or carbon atoms might have been incorporated into the lattice of TiO_2 by replacing titanium atoms in the form of Ti–O–C structure [24]. It has been reported that carbonate species formed on the TiO_2 surface could serve as the photosensitizer like organic dyes to increase the absorption ability of TiO_2 for visible light [10]. In our study, with the increase of solvothermal temperature, it was clear that carbonate species on the surface gradually decreased and disappeared in sample CN-TiO_2(160/300). In addition, one peak at ca. 281.3 eV can be found in both CN-TiO_2(120/300) and CN-TiO_2(160/300). The peak around 281 eV resulting from Ti–C bonds indicates that carbon substituted some of the oxygen atoms in the TiO_2 lattice [25]. It can be postulated that preferential Ti–C bonds

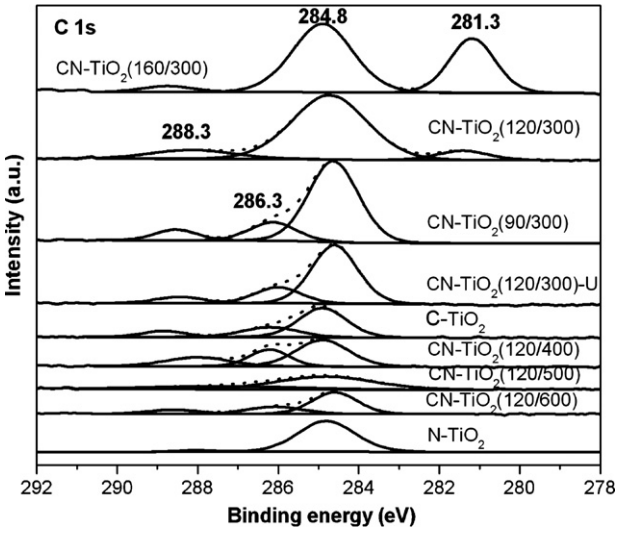

Fig. 2. High-resolution XPS spectra of C 1s core level for synthesized photocatalysts.

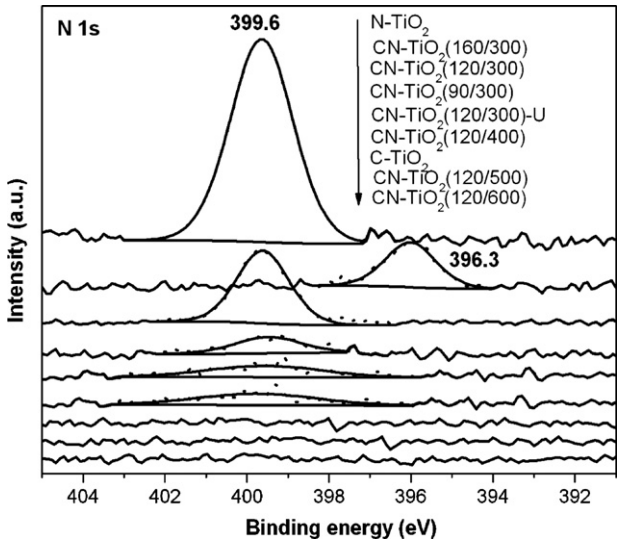

Fig. 3. High-resolution XPS spectra of N 1s core level for synthesized photocatalysts.

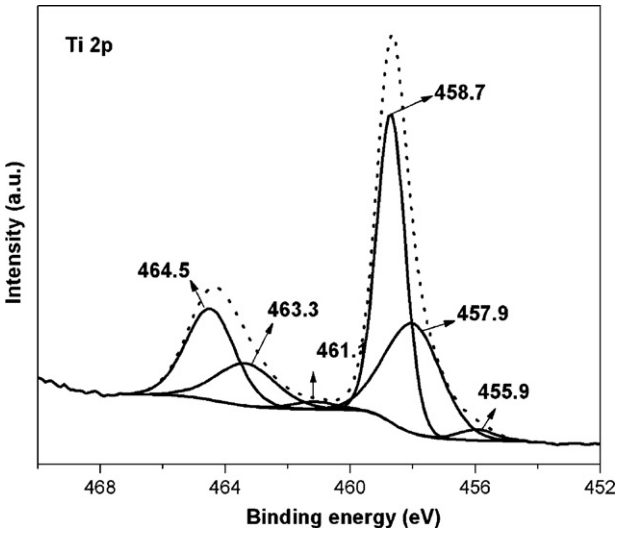

Fig. 4. High-resolution XPS spectra of Ti 2p core level for sample CN-TiO_2(120/300).

were thus formed at high solvothermal temperature. Under such solvothermal conditions, the atoms in crystal lattice vibrated drastically, even metastable TiO_2 surface might have been partially dissolved in solution causing rupture of Ti–O bonds. In the course of restructuring, C atoms might replace oxygen atoms in the crystal lattice [26,27]. On the other hand, the peak around 281 eV disappears and two shoulders around 286 and 288 eV become weaker with increasing calcination temperatures from 300 to 600 °C. This suggests that both Ti–C and Ti–O–C linkages tend to be destroyed by oxidation in air at high temperatures. Furthermore, only carbonate species were present on the surfaces of CN-TiO_2(120/300)–U and C-TiO_2, in contrast to that of CN-TiO_2(120/300). It is inferred that using HMT as the source of dopants strongly facilitates C substitution for O in the TiO_2 lattice. On the other hand, carbon content from the titanium precursor (TTIP) or solvent (isopropanol) might contribute to carbon doping of TiO_2 in the solvothermal method. For N-TiO_2, other than the peak at 284.8 eV, one peak corresponding to carbonate species is extremely weak. Hence N-TiO_2 was free of carbon dopant.

High-resolution N 1s spectra of as-prepared samples are shown in Fig. 3. One peak at 396.3 eV is only observed in CN-TiO_2(160/300). Most of the references attribute the N 1s peak positioned at 396 eV to Ti–N–Ti linkage, indicating that N atom is substitutionally doped into the TiO_2 lattice [28,29]. One peak at ca. 399.6 eV is shared by the other samples, which reveals the presence of oxynitride such as Ti–N–O and Ti–O–N on the surface [30,31]. The above results show that nitrogen and carbon atoms have been doped into TiO_2 of the surface of photocatalysts in the case of CN-TiO_2(120/300), CN-TiO_2(160/300), CN-TiO_2(90/300), CN-TiO_2(120/400) and CN-TiO_2(120/300)-U, while single dopant was found in the samples CN-TiO_2(120/500), CN-TiO_2(120/600), and C-TiO_2 and N-TiO_2.

The high-resolution XPS spectra of Ti 2p and O 1s core levels for CN-TiO_2(120/300) are shown in Figs. 4 and 5 respectively. Best fit of the Ti 2p XPS envelope resulted in three peaks at 464.5–461.1 eV for Ti $2p_{3/2}$ and three peaks at 458.7–455.9 eV for Ti $2p_{1/2}$. The peaks at 464.5 eV for Ti $2p_{3/2}$ and 458.7 eV for Ti $2p_{1/2}$ can be assigned to TiO_2 [32]. The other two pairs of Ti 2p peaks of lower binding energies may be due to the presence of Ti–N–O, Ti–O–N, and Ti–C linkages [33,34]. Three peaks at 528.5, 529.8 and 531.6 eV can be observed in O 1s XPS spectra. The peaks at 528.5 and 529.8 eV are ascribed to the Ti–O bonds [30], whilst the peak at 531.5 eV reveals that O atoms are bond to N or C in the form of carbonate species or oxynitrides [30]. Therefore, the chemical states of photocatalyst CN-TiO_2(120/300) could be confirmed by cross comparison of the XPS spectra of Ti 2p, O 1s, N 1s and C 1s.

3.2. Thermogravimetric analysis

Fig. 6 exhibits the weight loss events of the CN-TiO_2(120/T_2) precursor dried at 90 °C during heating in the air. Only one distinct step occurred at 49–124 °C, mainly ascribed to the loss of surface-adsorbed water or CO_2 molecules. No other peaks can be observed in DTG curve. It is known that the thermal decomposition of HMT become significant above 270 °C. Thus, it could be proposed that there was no residual HMT remaining in the sample CN-TiO_2(120/300) or at least the content of HMT residue was not detectable after solvothermal process. As shown in the TG curve, the major weight loss of 16.9% occurred below 300 °C, the subsequent weight loss of 2.8% happened at 300–600 °C, and the stable weight of sample can be observed at 600 °C and above. The minor decrease of weight at 300–600 °C could have been resulted from the loss of small amount of carbon or/and nitrogen species on the surface of TiO_2 during the heating process, because nitrogen or carbon tend to be replaced by oxygen in the air with the increasing temperature. This finding is in good agreement with the estimated atomic

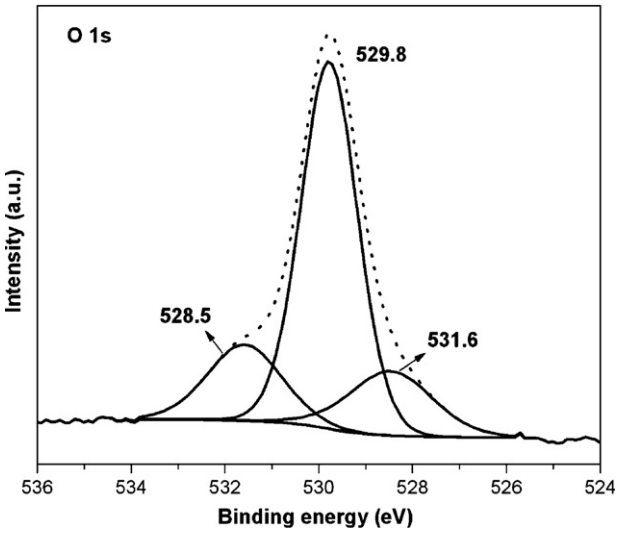

Fig. 5. High-resolution XPS spectra of O 1s core level for sample CN-TiO_2(120/300).

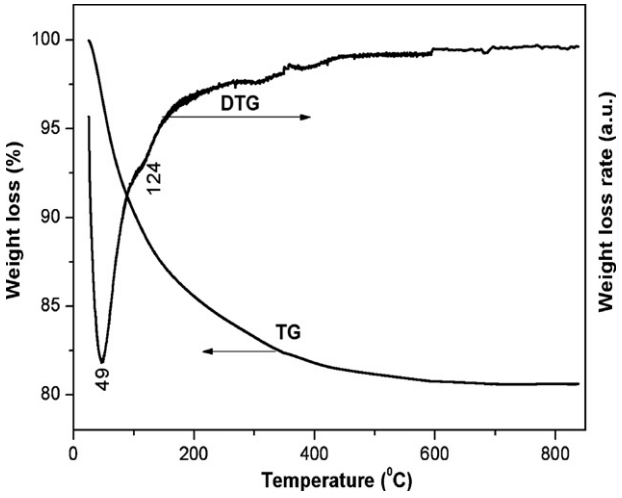

Fig. 6. TG/DTG profiles of the CN-TiO_2(120/T_2) precursor dried at 90 °C.

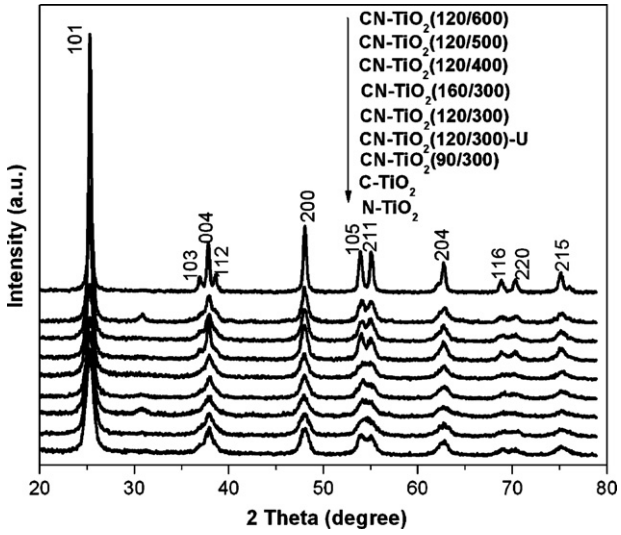

Fig. 7. XRD patterns of synthesized photocatalysts.

concentrations of C and N of the samples CN-TiO_2(120/T_2) calcined at different temperatures (Table 1).

3.3. Structure and textural properties

The XRD patterns of all photocatalysts are of well-developed anatase phase (Fig. 7). No rutile phase was found even after calcination at 600 °C. For the samples calcined at elevated temperatures, the diffraction peaks become sharper and stronger. These observations indicate the crystallite size could be increased and the crystallinity of anatase TiO_2 could be improved with the increasing calcination temperature; the solvothermal synthesis was more favorable in synthesizing fine particles of high crystallinity. On the other hand, the existence of dopants might enhance the thermal stability of TiO_2. The crystallite sizes of all the samples as estimated using Scherrer equation are shown in Table 1 while the morphologies of the CN-TiO_2(120/300) and C-TiO_2 are compared in Fig. 8. It is obvious that modification with carbon and nitrogen using HMT and urea could increase the particle sizes as compared to the TiO_2(120/300).

The BET specific surface area, pore size and pore volume of derived photocatalysts are listed in Table 1. Obviously, the preparation conditions would influence the specific surface area and pore volume of the product. The surface areas for the samples calcined at 300 °C (92–156 m^2/g) were much higher than that of P25, and gradually declined with increasing calcination temperature due to thermal destruction of the mesoporous structure under high temperatures. The nitrogen adsorption/desorption isotherm for CN-TiO_2(120/300) (data not shown here) can be classified as a Type IV isotherm based on IUPAC classification with hysteresis loops, which is typical of a mesoporous material [35]. The pore size distribution curve calculated from the desorption branch of nitrogen isotherm by Barrett–Joyner–Halenda (BJH) method shows that the interparticle pore diameter falls in the range of 5–11 nm. The well-developed mesoporosity, large surface area, and 3D interconnected pore architecture could improve molecular transport of reactants and products to achieve high PCD efficiency.

3.4. Optical properties

UV-vis diffuse reflectance spectra (DRS) of the selected as-prepared photocatalysts and P25 are shown in Fig. 9. In general, the spectra of prepared photocatalysts exhibit the remarkable red shift of absorption edge to the visible-light region with long band tailings. Based on the optical adsorption edge obtained from the DRS, the respective energy band gaps were calculated by the transformed Kubelka–Munk function [36], as shown in Table 1. CN-TiO_2(120/300) displayed the lowest band gap owing to the synergistic coexistence of Ti–C, Ti–C–O, Ti–O–C, Ti–N–O, and Ti–O–N

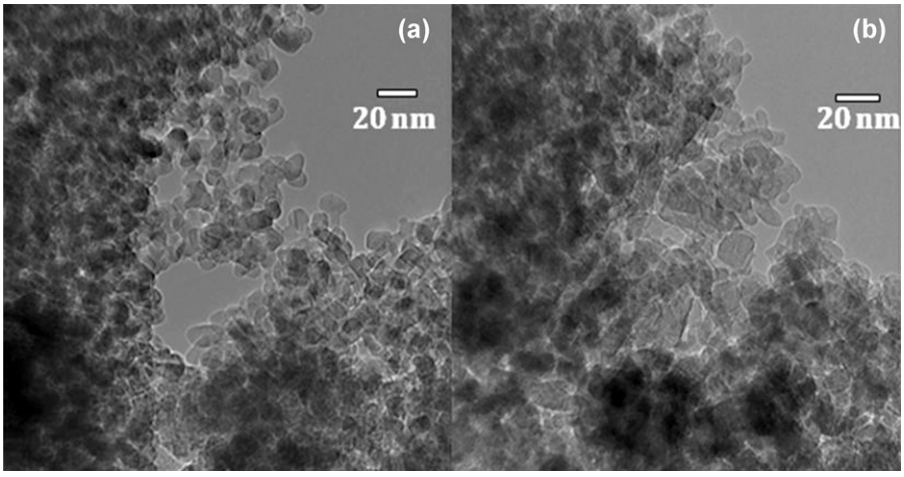

Fig. 8. TEM images of (a) C-TiO_2, and (b) CN-TiO_2(120/300).

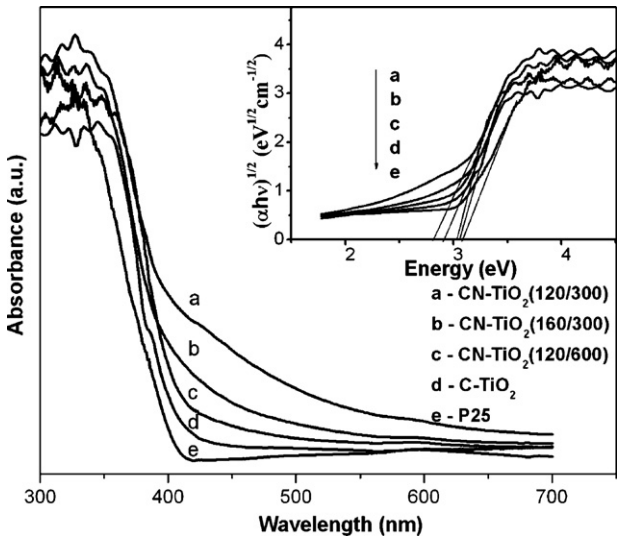

Fig. 9. UV–vis diffuse reflectance spectra of the photocatalysts. Inset shows the corresponding Kubelka–Munk transformed reflectance spectra.

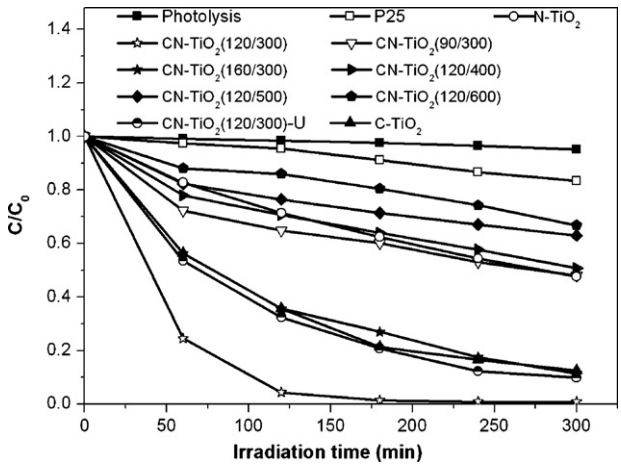

Fig. 10. Photodegradation of BPA over various photocatalysts under white LED irradiation at neutral pH.

linkages. The origin of the adsorption edge's red shift is hitherto controversial. Some studies have proposed that it is caused by a narrowing band gap via a mixed C or N 2p state with O 2p state in the valence band, while others have suggested the appearance of intragap localized states of dopants [37]. Additionally, a point was raised about the formation of oxygen vacancies and the emerged color centers which could contribute to absorb visible light [38]. For the sample CN-TiO_2(120/300), on the basis of above-mentioned XPS analysis, it is possible that the narrowing band gap, resulted from mixed C and/or N 2p with O 2p states, and the intragap localized states of C and/or N together contribute to the red shift of the absorption edge. The presence of lattice disorder is thought to result in the extended tailing. In addition, visible-light absorbance depended on the preparation conditions, which resulted in varying amounts of N and C doping in TiO_2. This observation is consistent with the XPS results shown earlier. Furthermore, the adsorption onset for the sample CN-TiO_2(120/300) extended up to 600 nm, which implies that the photocatalyst could be visible-light active even under yellow light.

3.5. Photocatalytic degradation

3.5.1. Comparison of photocatalytic performance over various photocatalysts

Fig. 10 shows the PCD of BPA with various synthesized photocatalysts and P25 under white LED irradiation at neutral pH. The corresponding BPA and TOC removal efficiencies are summarized in Table 1. It was found that photolysis could induce only 3% degradation of BPA after 5 h. In general, the photocatalysts prepared under solvothermal conditions exhibited significantly improved PCD efficiencies compared to that of P25. In particular, CN-TiO_2(120/300) exhibited higher efficiencies of BPA degradation and mineralization than any of the other prepared photocatalysts. The BPA was degraded to 96% within the initial 2 h, and completely removed after 5 h of irradiation. Concomitantly, the about 70% of organic carbon (measured as TOC) was completely mineralized after 5-h irradiation, of which the remaining 30% might be attributed to the formation of recalcitrant intermediates as reported in previous literature [22,39].

It is postulated that the photocatalytic performance would be governed by the following factors. First, the lattice defects, arising from the C and/or N modification, would be critical for the visible-light photocatalysis. It is also known that the lattice impurities could inhibit recombination of the photoinduced electrons and holes, leading to the increased quantum efficiency [40]. Second, the active sites play an important role in the photocatalytic process. The mesoporous system with high surface area is favorable for the diffusion and adsorption of BPA molecules. Additionally, the well-formed anatase phase obtained via solvothermal treatment may benefit the photodegradation of BPA. The synergistic effects of carbon and nitrogen codoping into TiO_2 resulted in higher photoactivity of CN-TiO_2(120/300) than C-TiO_2 and N-TiO_2, which, on the contrary, were only C or N-modified but possessed the larger BET surface areas (156 and 143 m^2/g). Owing to the combined promotion from solvothermal treatment and incorporation of N and C dopants into the TiO_2 lattice of the surface, CN-TiO_2(120/300) exhibited the highest efficiencies for both BPA photodegradation and mineralization under the Vis-LED irradiation. According to the above results, the following sections specifically discuss the performance of CN-TiO_2(120/300) in the Vis-LED photoreactor.

3.5.2. Photocatalytic degradation kinetics

BPA photodegradation in aqueous CN-TiO_2(120/300) suspension likely involved a number of steps similar to conventional heterogeneous photocatalytic reactions, First, BPA molecules diffused into the surface and pores of CN-TiO_2(120/300), reached active sites where hydroxyl radicals were generated. Degradation products (intermediates or CO_2) were subsequently formed and adsorbed on the interface. Finally, the products desorbed from the interface and diffused away from the solid surface. The interaction of hydroxyl radicals with BPA is thought to be a rate-limiting step. Langmuir–Hinshelwood model can be used to describe these processes, in which the reaction rate (r) is a function of the degree of substrate coverage (θ):

$$r = k\theta = k\left(\frac{KC}{1+KC}\right) \quad (1)$$

where C is the BPA concentration, k is the intrinsic reaction rate constant, and K is the Langmuir adsorption equilibrium constant. In this study, the low BPA concentration (initial $C \approx 0.02$ mM) and the weak affinity of titania for a non-polar organic suggest that $KC \ll 1$. Hence, pseudo-first-order reaction kinetics can be assumed:

$$r = -\frac{dC}{dt} = kKC = k_{ap}C \quad (2)$$

where k_{ap} represents the apparent degradation rate constant. The k_{ap} values are summarized in Table 2.

Table 2
Kinetic constants and PCD efficiencies using CN-TiO_2(120/300) at various reaction conditions.

Experimental condition			k_{ap} ($\times 10^{-3}$ min^{-1})	R^2	PCD at 5 h (%)
Light	pH	Anion			
White (P25)	6.2 ± 0.1	–	0.5	0.976	15
White	6.3 ± 0.1	–	25	0.998	>99
Blue	6.3 ± 0.1	–	21	0.987	>99
Green	6.4 ± 0.1	–	6	0.998	84
Yellow	6.3 ± 0.1	–	0.8	0.994	24
White	3.1 ± 0.1	–	9	0.996	95
White	5.2 ± 0.1	–	15	0.998	98
White	9.1 ± 0.1	–	18	0.994	>99
White	11.1 ± 0.1	–	5	0.991	80
White	6.2 ± 0.1	Cl^- (5.0 mM)	15	0.998	>99
White	6.8 ± 0.1	NO_3^- (5.0 mM)	16	0.991	>99
White	6.4 ± 0.1	SO_4^{2-} (5.0 mM)	17	0.994	>99
White	6.5 ± 0.1	HCO_3^- (5.0 mM)	4	0.986	67
White	6.5 ± 0.1	HCO_3^- (1.5 mM)	9	0.986	84
White	6.5 ± 0.1	HCO_3^- (0.3 mM)	22	0.986	98
White	6.8 ± 0.1	Silica (5.0 mM)	2	0.970	50
White	6.8 ± 0.1	Silica (1.5 mM)	11	0.970	90
White	6.8 ± 0.1	Silica (0.3 mM)	23	0.970	99
White	3.2 ± 0.1	Silica (5.0 mM)	12	0.970	91
White	5.0 ± 0.1	Silica (5.0 mM)	5	0.970	74
White	9.0 ± 0.1	Silica (5.0 mM)	1.5	0.970	39

3.5.3. Action spectra of the photocatalyst

Fig. 11 shows the results of PCD of BPA using CN-TiO_2(120/300) under different colors of Vis-LED irradiations at neutral pH, while their PCD rates are compared in Table 2. The PCD efficiencies of BPA could reach up to >99%, >99%, 84% and 24% under 5-h irradiation of white, blue, green, and yellow LEDs, respectively. The corresponding extents of TOC removal were 70%, 60%, 45% and 9%, respectively. Without CN-TiO_2(120/300), only up to 3% of BPA could be degraded via photolysis. For CN-TiO_2(120/300), it is hypothesized that there were more valence-band electrons photoexcited to conduction band under white light irradiation, as white LED emits blue light of about 450 nm and broadband light of around 500–600 nm. Under long-wavelength of yellow LED irradiation, the catalyst was still able to remove a small fraction of BPA. Apparently, C–N codoping could extend the adsorption edge of CN-TiO_2(120/300) to about 600 nm.

3.5.4. Effect of initial pH

Effect of initial pH on BPA degradation over CN-TiO_2(120/300) under white LED irradiation is presented in Fig. 12, and the corresponding rate constants are shown in Table 2. The order of degradation rates follows pH 7 > pH 9 ≈ pH 5 > pH 3 > pH 11. Apparently the circumneutral condition is the most favorable for PCD of BPA by the CN-TiO_2(120/300). There are two determining factors leading to the observed trend, namely, the adsorption mode of BPA on photocatalyst surface and the formation of hydroxyl radicals. It is known that TiO_2 is amphoteric in aqueous solution. The point of zero charge (pzc) of C and N codoped TiO_2 was found to be at pH 5.29. Thus surface of TiO_2 is positively charged at a low pH (<pH_{pzc}), and negatively charged at a higher pH (>pH_{pzc}). On the other hand, BPA molecules possess two negative oxygen atoms at the hydroxyl groups and four negative carbon atoms ortho to the phenolic group. Additionally, BPA has the pK_{a1} and pK_{a2} values of approximately 9.6 and 10.2, respectively [41]. Increasing deprotonation of BPA into BPA^- and BPA^{2-} occurred when pH was raised to >9. Therefore, BPA appeared to be attracted to the positively charged surface of CN-TiO_2(120/300) at pH ≤5, while repelled at higher pH (pH ≥7). The postulation is in good agreement with the BPA adsorption capacities of CN-TiO_2(120/300) at corresponding pH, as shown in the inset of Fig. 12. Meanwhile, with the increase of

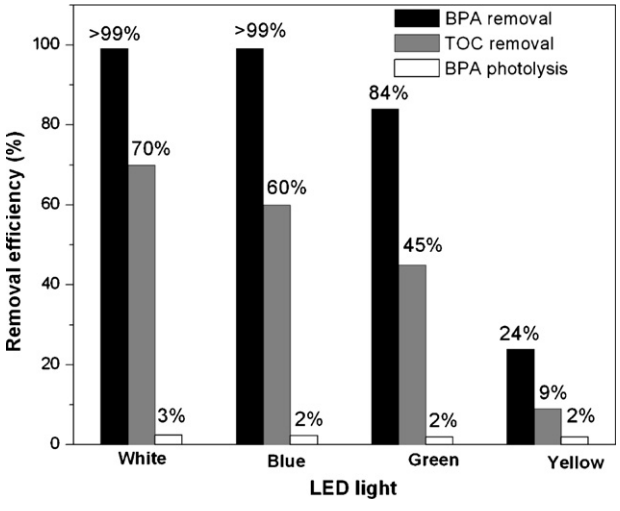

Fig. 11. BPA photolysis and photodegradation by CN-TiO_2(120/300) under different Vis-LED irradiation for 5 h at neutral pH.

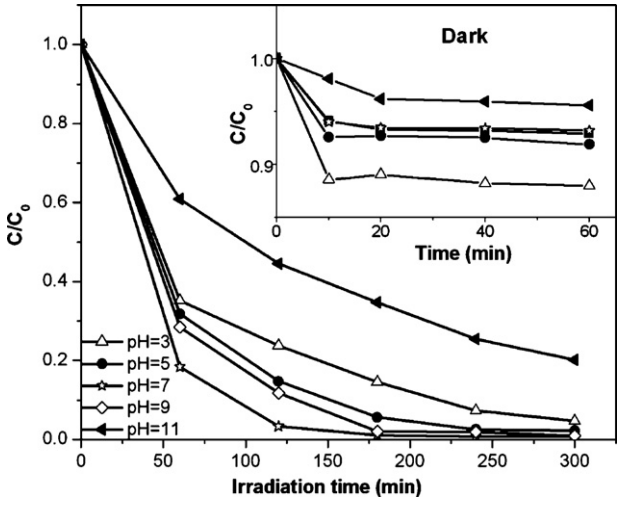

Fig. 12. Effect of pH on photocatalytic degradation of BPA over CN-TiO_2(120/300) under white LED irradiation. Inset shows the corresponding results for BPA adsorption in dark within 1 h.

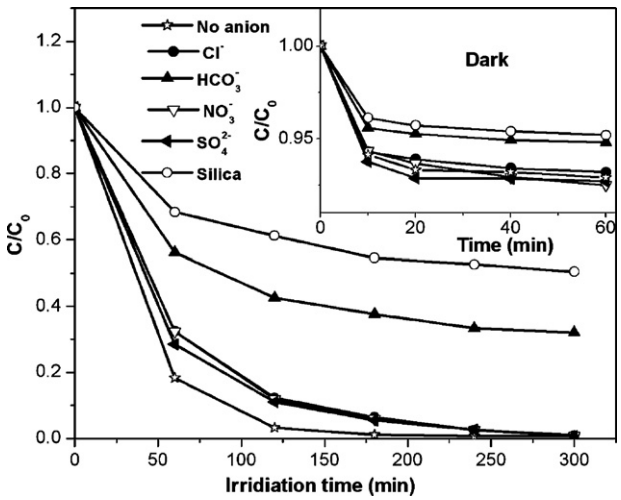

Fig. 13. Effect of common anions at 5.0 mM on photocatalytic degradation of BPA over CN-TiO_2(120/300) under white LED irradiation at neutral pH. Inset shows the corresponding results for BPA absorption in dark within 1 h.

pH, a higher concentration of hydroxyl radicals could be generated. The increased generation of hydroxyl radicals in alkaline conditions enhanced photocatalytic activities, while the repulsion effect of BPA molecules from the surface of CN-TiO_2(120/300) at high pH levels (pH > pK_{a1}) was deemed inhibitory to PCD. Apparently, these two factors are conflicting with respect to BPA photodegradation. There is an optimum condition for photodegradation of BPA at circumneutral pH (between 5 < pH < 9).

3.5.5. Effect of anions

For practical application of photocatalysis in water and wastewater treatment, it is imperative to investigate the influence of common matrix species in the aqueous systems on the degradation of the target pollutant. Inorganic anions such as chloride, nitrate, sulfate, bicarbonate, and silica are prevalent in surface waters, groundwaters and wastewaters. The anions generally exhibited varying degrees of inhibitory effects on photocatalytic activities of CN-TiO_2(120/300), with the orders of significance following silica > bicarbonate > chloride > nitrate > sulfate at 5.0 mM, as shown in Table 2 and Fig. 13. In general, the presence of sulfate, nitrate, and chloride only caused marginal reduction in BPA removal efficiencies. However, silica and bicarbonate could inhibit the PCD process to a much larger extent. Interestingly, the detrimental effects caused by silica and bicarbonate became insignificant at a lower concentration of <1.5 mM which encompasses their typical background concentration levels in surface waters, groundwater, and wastewaters. The inhibitory effects at high anion concentrations might be generally due to two plausible phenomena. First, the anions could compete with BPA for active sites of adsorption on the surface of photocatalyst, since their concentrations (5.0 mM) are far beyond that of BPA (5 ppm or 0.02 mM). In addition, anions such as chloride, nitrate, sulfate, and bicarbonate have been reported to scavenge •OH and form ionic radicals, such as Cl•, NO_3•, SO_4•$^-$ and HCO_3•/CO_3•$^-$ (Eqs. (3)–(5)), which are less reactive than •OH [42,43].

$$\bullet OH + (Cl^-,\ NO_3^-,\ SO_4^{2-} \text{ and } HCO_3^-) \rightarrow (Cl\bullet,\ NO_3\bullet,\ SO_4\bullet^- \text{ and } HCO_3\bullet) + OH^- \quad (3)$$

$$h_{vb}^+ + (Cl^-,\ NO_3^-,\ SO_4^{2-} \text{ and } HCO_3^-) \rightarrow (Cl\bullet,\ NO_3\bullet,\ SO_4\bullet^- \text{ and } HCO_3\bullet) \quad (4)$$

$$\bullet OH + HCO_3^- \rightarrow CO_3\bullet^- + H_2O \quad (5)$$

Therefore, the excess existence of anions would inevitably inhibit the photodegradation of BPA to a certain extent.

For bicarbonate (5.0 mM), the more noticeable inhibitory effect might be explained as follows. Bicarbonate could be irreversibly adsorbed on the photocatalyst surface by generating of a negatively charged layer, while sulfate, nitrate, and chloride anions would be attracted to the surface of photocatalyst via hydrogen bridges and Van der Waals interactions whereby the adsorption is reversible [43,44]. This hypothesis was supported by studying the adsorption of BPA in the presence of these anions. In our experiments, BPA was less adsorbed at equilibrium in the existence of bicarbonate than in the existence of sulfate, nitrate, and chloride, as shown in the inset of Fig. 10. Furthermore, it has been reported that bicarbonate could trap the hydroxyl radicals with a comparatively higher second-order constant of $3.9 \times 10^8\ M^{-1}\ S^{-1}$ to produce carbonate radicals which is mainly a selective electrophilic reagent and is less reactive than hydroxyl radicals [45,46].

Dissolved silica is naturally present in aquatic environment due to dissolution of many minerals and rocks over a large part of earth's surface. The silica content of water ranges from a few ppm in surface supplies to over 100 ppm in certain groundwater. Unlike most oxyanions, silica can undergo polymerization at relatively low concentration, leading its rather complex solution chemistry [47]. Hence, an understanding of silica effect is of practical importance when evaluating photocatalysis in aqueous system. This study found that at pH 7, silica concentration of 1.5 mM only caused a minor reduction in the photocatalytic removal of BPA compared to when no silica is present. However, at 5.0 mM, the reduction in PCD was pronounced. The inhibitory effect was highly pH-dependent. It was more noticeable with increasing pH. At pH 3, even in the presence of 5.0 mM, the removal efficiency of BPA could achieve up to 91% after 5 h irradiation, compared to 74% at pH 5, 50% at pH 6.8, and 39% at pH 9. The rate constants for the reaction in acid conditions are also significantly higher than those at neutral and alkaline conditions (Table 2). Therefore, reducing the pH of the water prior to photocatalysis treatment may therefore be an effective option for improving BPA removal in the presence of high concentrations of silica. These findings can be attributed to the unique characteristics of dissolved silica in solution. At concentrations below its solubility limit (2 mM for amorphous silica), dissolved silica is dominantly present as monomeric species $SiO_2(OH)_2^{2-}$, SiO_3^{2-} or $Si(OH)_4$ at different pH [48]. Silica acid is predominant in the solution at neutral or acidic pH. These neutral molecules have relatively weak affinity to the CN-TiO_2(120/300) surface. Therefore, the inhibition of BPA photodegradation was drastically suppressed under acid conditions. At higher concentration, the silica speciation in aqueous phase becomes more complex. Polymeric or colloidal silica may form by condensation of monomers [48,49]. It might be associated with surface hydroxyl functional group leading to the formation of surface-bound silica polymers and silica multilayers. As a result, when silica was at the concentration of 5.0 mM, the active sites of photocatalysts might be blocked and the light could be intercepted by colloidal or/and polymeric silica surrounding the photocatalysts. The existence of the surface-bond silica species was also confirmed by XPS and FTIR spectra of CN-TiO_2(120/300) obtained before and after the BPA photodegradation experiments, as shown in Figs. 14 and 15 respectively. FTIR studies were carried out using Perkin-Elmer 2000 spectrophotometer. The peak at around 102.0 eV of the XPS spectra attributable to Si–O bonds (Fig. 14) can be observed for the samples exposed to 5.0 mM silica at different pH. It reveals the presence of silica-based linkages on the surface of the photocatalyst. Similarly, the presence of silica polymers was also detected based

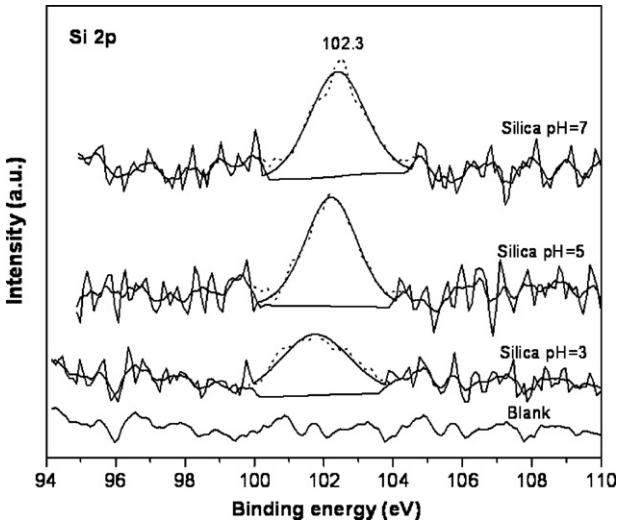

Fig. 14. High-resolution XPS spectra of Si 2p core level for CN-TiO_2(120/300) after photocatalytic reaction in the presence of silica at various pH (blank represents CN-TiO_2(120/300) before exposure to silica).

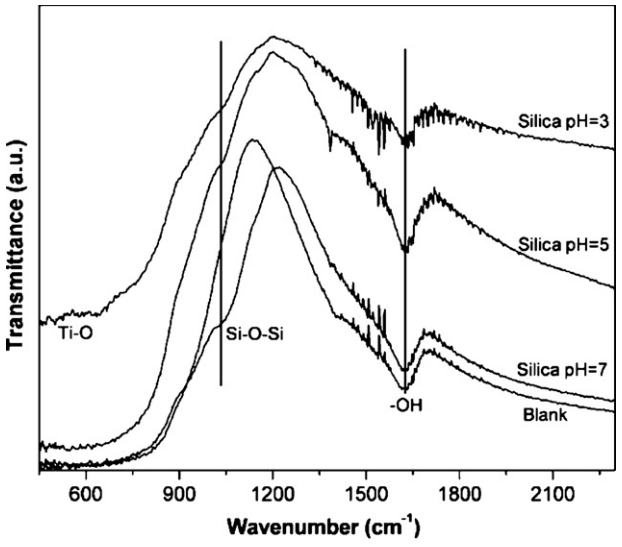

Fig. 15. FTIR spectra of CN-TiO_2(120/300) after photocatalytic reaction in the presence of silica at various pH (blank represents CN-TiO_2(120/300) before exposure to silica).

on the appearance of peak located at about 1050 cm^{-1} (Fig. 15), which is associated with asymmetric Si–O–Si stretching vibrations [48].

4. Conclusions

Several visible-light photoactive C–N codoped TiO_2 were prepared by a facile solvothermal method. The photocatalysts generally exhibited improved PCD efficiencies compared to that of P25. Owing to synergistic effects of carbon and nitrogen codoping into TiO_2 and large BET surface area, the CN-TiO_2(120/300) showed the highest efficiencies for both BPA degradation and mineralization under LED irradiation. Since the absorption onset of this C–N codoped TiO_2 can extend to about 600 nm, high efficiencies of BPA degradation were also achieved after 5-h irradiation of blue and green light. Presence of chloride, nitrate, and sulfate appeared to only slightly inhibit the BPA degradation by C–N codoped TiO_2. While silica and bicarbonate can have adverse effect on PCD of BPA, the detrimental influences became insignificant at a lower concentration (<1.5 mM). XPS and FTIR revealed that this deactivation was linked to formation of surface-bound silica species. Pretreatment of the solution by simply reducing the pH can prevent deactivation of the C–N codoped TiO_2 by silica. This work signifies the potential application of carbon and nitrogen codoped TiO_2 synthesized via solvothermal route in pollutant removal under sunlight irradiation. While in the absence of sunlight, LEDs with versatile configuration provides potential for optimized optical solution such as uniform illumination, inherent compactness, and higher photon efficiency in photoreactor systems.

Acknowledgement

The National Research Foundation (NRF) of Singapore is hereby acknowledged for the financial support through the project EWI RFP 0802-11, which aims to develop novel photocatalysts for water purification using solar light.

References

[1] J.M. Herrmann, Catal. Today 53 (1999) 115–129.
[2] H. Irie, Y. Watanabe, K. Hashimoto, Chem. Lett. 32 (2003) 772–773.
[3] R. Bacsa, J. Kiwi, T. Ohno, P. Albers, V. Nadtochenko, J. Phys. Chem. B 109 (2005) 5994–6003.
[4] G. Wu, J. Wang, D.F. Thomas, A. Chen, Langmuir 24 (2008) 3503–3509.
[5] C. Belver, R. Bellod, A. Fuerte, M. Fernandez-Garcia, Appl. Catal. B 65 (2006) 301–308.
[6] X.B. Chen, C. Burda, J. Am. Chem. Soc. 130 (2008) 5018–5019.
[7] D. Li, N. Ohashi, S. Hishita, T. Kolodiazhnyi, H. Haneda, J. Solid State Chem. 178 (2005) 3293–3302.
[8] M. Pelaez, A.A. de la Cruz, E. Stathatos, P. Falaras, D.D. Dionysiou, Catal. Today 144 (2009) 19–25.
[9] E.A. Reyes-Garcia, Y. Sun, D. Raftery, J. Phys. Chem. C 111 (2007) 17146–17154.
[10] D. Chen, Z. Jiang, J. Geng, Q. Wang, D. Yang, Ind. Eng. Chem. Res. 46 (2007) 2741–2746.
[11] S. Yin, K. Ihara, Y. Aita, M. Komatsu, T. Sato, J. Photochem. Photobiol. A 179 (2006) 105–114.
[12] Y. Huo, Y. Jin, J. Zhu, H. Li, Appl. Catal. B 89 (2009) 543–550.
[13] X. Chen, S.S. Mao, Chem. Rev. 107 (2007) 2891–2959.
[14] Z. Jiang, F. Yang, N. Luo, B.T.T. Chu, D. Sun, H. Shi, T. Xiao, P.P. Edwards, Chem. Commun. (2008) 6372–6374.
[15] H. Li, J. Li, Y. Huo, J. Phys. Chem. B 110 (2006) 1559–1565.
[16] S. Yin, Y. Aita, M. Komatsu, J.S. Wang, Q. Tang, T. Sato, J. Mater. Chem. 15 (2005) 674–682.
[17] D.G. Huang, S.J. Liao, J.M. Liu, Z. Dang, L. Petrik, J. Photochem. Photobiol. A 184 (2006) 282–288.
[18] J.P. Ghosh, C.H. Langford, G. Achari, J. Phys. Chem. A 112 (2008) 10310–10314.
[19] A.V. Krishnan, P. Stathis, S.F. Permuth, L. Tokes, D. Feldman, Endocrinology 132 (1993) 2279–2286.
[20] J. Jackson, R. Sutton, Sci. Total. Environ. 405 (2008) 153–160.
[21] K. Nomiyama, T. Tanizaki, T. Koga, K. Arizono, R. Shinohara, Arch. Environ. Contam. Toxicol. 52 (2007) 8–15.
[22] Y. Ohko, I. Ando, C. Niwa, T. Tatsuma, T. Yamamura, T. Nakashima, Y. Kubota, A. Fujishima, Environ. Sci. Technol. 35 (2001) 2365–2368.
[23] N. Watanabe, S. Horikoshi, H. Kawabe, Y. Sugie, J. Zhao, H. Hidaka, Chemosphere 52 (2003) 851–859.
[24] W. Ren, Z. Ai, F. Jia, L. Zhang, X. Fan, Z. Zou, Appl. Catal. B 69 (2007) 138–144.
[25] L. Zhang, R.V. Koka, Mater. Chem. Phys. 57 (1998) 23–32.
[26] L.B. Kriksunov, D.D. Macdonald, J. Electrochem. Soc. 142 (1995) 4069–4073.
[27] C.C. Tsai, H. Teng, Chem. Mater. 16 (2004) 4352–4358.
[28] H. Irie, Y. Watanabe, K. Hashimoto, J. Phys. Chem. B 107 (2003) 5483–5486.
[29] R. Asahi, T. Morikawa, T. Ohwaki, K. Aoki, Y. Taga, Science 293 (2001) 269–271.
[30] C. Chen, H. Bai, C. Chang, J. Phys. Chem. C 111 (2007) 15228–15235.
[31] X. Chen, Y. Low, A.C.S. Samia, C. Burda, J.L. Gole, Adv. Funct. Mater. 15 (2005) 41–49.
[32] N.C. Saha, H.G. Tompkins, J. Appl. Phys. 72 (1992) 3072–3079.
[33] X. Chen, C. Burda, J. Phys. Chem. B 108 (2004) 15446–15449.
[34] L.H. Zhang, R.V. Koka, Mater. Chem. Phys. 57 (1998) 23–32.
[35] K.S.W. Sing, D.H. Everett, R.A.W. Haul, L. Moscou, R.A.I. Pierott, J. Rouquerol, T. Siemieniewska, Pure Appl. Chem. 57 (1985) 603–619.
[36] N. Serpone, D. Lawless, R. Khairutdinov, J. Phys. Chem. 99 (1995) 16646–16654.
[37] C. Di Valentin, G. Pacchioni, A. Selloni, S. Livraghi, E. Giamello, J. Phys. Chem. B 109 (2005) 11414–11419.
[38] N. Serpone, J. Phys. Chem. B 110 (2006) 24287–24293.
[39] K. Chiang, T.M. Lim, L. Tsen, C.C. Lee, Appl. Catal. A 261 (2004) 225–237.
[40] A.L. Linsebigler, G. Lu, J.T. Yates Jr., Chem. Rev. 95 (1995) 735–758.
[41] P.G. Kosky, J.M. Silva, E.A. Guggenheim, Ind. Eng. Chem. Res. 30 (1991) 462–467.
[42] R.A. Burns, J. Environ. Eng. 125 (1999) 77–85.
[43] A.G. Rincoĭn, C. Pulgarin, Appl. Catal. B 51 (2004) 283–302.

[44] C. Hu, T. Yuchao, L. Lanyu, H. Zhengping, W. Yizhong, T. Hongxiao, J. Chem. Technol. Biotechnol. 79 (2004) 247–252.
[45] I. Gultekin, N.H. Ince, J. Environ. Sci. Health. Part A Environ. Sci. Health Part A Environ. Sci. Eng. 39 (2004) 1069–1081.
[46] C. Guillard, E. Puzenat, H. Lachheb, A. Houas, J.M. Herrmann, Int. J. Photoenergy 7 (2005) 1–9.
[47] T.P. Luxton, M.J. Eick, D.J. Rimstidt, Chem. Geol. 252 (2008) 125–135.
[48] X.F. Yang, P. Roonasi, A. Holmgren, J. Colloid Interface Sci. 328 (2008) 41–47.
[49] T. Kohn, S.R. Kane, D.H. Fairbrother, A.L. Roberts, Environ. Sci. Technol. 37 (2003) 5806–5812.